感覚神経系障害患者のための ウェアラブル感覚補填・感覚強化システムの開発
～マイクロスティミュレーション法による触圧覚生成と感覚増強～

Wearable sensory prosthetic system for patients with sensory disturbance
-generation of somatic sensation and its enhancement using microstimulation method-

○新納 弘崇 (電通大)　國本 雅也 (済生会横浜市東部病院)　鈴木 隆文 (東京大)　満渕 邦彦 (東京大)　下条 誠 (電通大)

Hirotaka Niiro(UEC),Masanari Kunimoto(Saiseikai Hosp.),Takafumi Suzuki(Univ. of Tokyo),
Kunihiko Mabuchi(Univ. of Tokyo),Makoto Shimojo(UEC)

Abstract— In this study, we attempted to develop a prototype of a wearable sensory prosthetic system with which patients suffering from peripheral sensory disturbance will be able to feel somatic sensations as if they were touching an object with their healthy and intact hand. The system consists of finger sacs and palm patch equipped with flexible pressure sensors, and micro-electrical stimulation of the sensory nerve fibers was used in order to evoke somatic sensations. The results showed that the system worked satisfactorily, and it is demonstrated that the system will be able to compensate or even enhance sensory function of the patients with sensory neuropathy.

Key Words: sensory feedback,intelligent prosthetic hand,work support,microstimulation method

1. 緒言

病気や事故によって感覚を失ってしまった場合，日常生活に多大な支障をきたす事になる．そこで，障害によって失った感覚を回復するための一つの方法として，感覚神経電気刺激を利用した感覚を提示する研究がなされるようになった [1].

実際の生体では，感覚受容器が受けた刺激を活動電位のパルス列に変換し，中枢に伝達されることで感覚を得る [2]. そして，刺激を伝える感覚神経線維に同じ活動電位列を発生させることができれば，実際に刺激を受けた時と同じ感覚を得ることができる.

そこで本研究では，触覚センサの情報をマイクロスティミュレーション法を用いて，感覚神経経由により触感覚として提示するシステムの開発を目的とした.

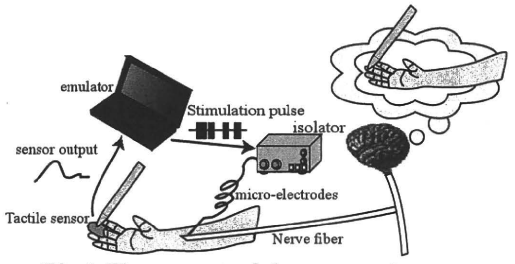

Fig.1 The concept of the proposed system.

2. 実験システム

実験システムの全体構成を図 2 に示す．システムは触覚センシングと神経線維インターフェースの 2 つに分かれている．前者は被験者の指先に装着した触覚センサの情報をコンピュータに取り込み，後者は取り込んだ情報に応じて神経線維を刺激するパルス列を出力する．以下各実験システムについて説明する.

2.1 触覚センサ

触覚センサとして FingerTPS(PPS 社製) を用いた．センサは人の手に装着し，接触力を検出するフレキシブルな静電容量型圧力センサである．出力は Bluetooth 通信で PC に接続され，40Hz で更新する.

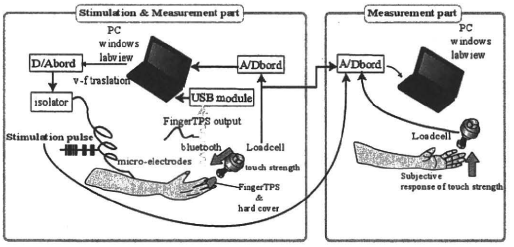

Fig.2 The experimental arrangement.

2.2 神経線維インターフェース

触覚センサからの情報を基にマイクロスティミュレーション法を用いて感覚を被験者に提示する．マイクロスティミュレーション法とは，経皮的に微小針電極を感覚神経線維の中に刺入し，電気刺激パルス列を入力することで，人工感覚を生成する手法である.

Fig.3 The Finger TPS system.

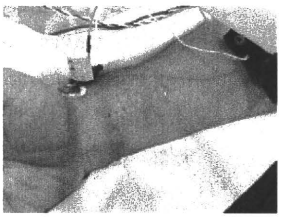

Fig.4 The manner in which microstimulation is performed.

3. 感覚提示実験

感覚神経への電気刺激によって生成される圧感覚の強度はパルス頻度に依存している [3] 事が報告されており，本研究ではこの関係を応用する．

3.1 実験目的・方法

本実験の被験者は，健全な男性 1 名である．被験者は座っており，開眼状態で実験を行った．指先に加えた力によって発生する感覚と等価な感覚量を感覚神経の電気刺激で発生させることを目的とする．この為には，指先に発生した感覚を定量評価する必要がある．今回我々は生成された感覚の計測法として，加圧した指先に発生される力と反対の指先でその力に対し等価な感覚量を提示させることとした．

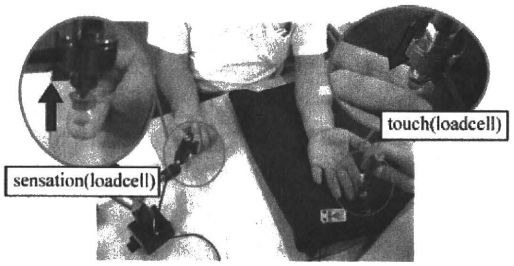

Fig.5 Quantitative evaluation of the pressure sensation evoked by microelectricqal stimulation.

3.2 機械刺激に対する感覚量

まず，片方の指先に力を加え，その力と同等の力を反対の指先で提示する実験を行った．実験結果を図 6 に示す．加圧力と感覚量の相関係数は 0.98 であり，相関が高いことから，皮膚表面に加えた機械刺激と感覚量の関係はほぼ等価な関係であることが示された．

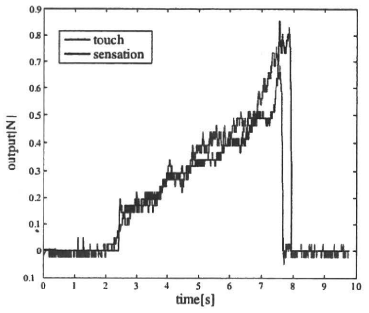

Fig.6 Actual force applied to the TPS sensor and the subjective magnitude of the evoked pressure sensation.

3.3 電気刺激に対する感覚量

次に，指先にハードカバーを装着し，感覚を遮断した状態で感覚を提示する実験を行った．FingerTPS の出力をパルス列頻度に変換・出力し，マイクロスティミュレーション法によりパルス列を神経に伝達することで感覚を提示した (図 7)．

本実験では，圧覚から電気刺激のパルス列頻度への変換式は，FingerTPS の出力 x を係数 a にて整数倍し，これをパルス頻度の周波数 f とした．即ち，$f = ax$ で，本実験では $a = 50$ とした．

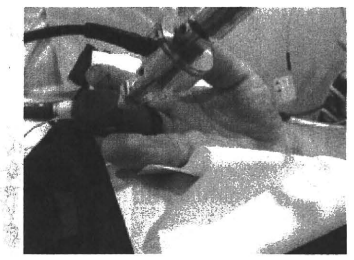

Fig.7 The manner in which a subject enhances somatic sensations by the developed system.

実験結果の一例を図 8 に示す．グラフは上から FingerTPS と加圧力と感覚量，出力周波数，出力パルスである．実験結果をみると，パルス頻度が増加することによって被験者の感覚量は増加している．押付力と感覚量の関係は相関係数 0.91 であり，高い相関があることから被験者の感覚を生成出来ていることがわかる．また，FingerTPS と押付力との相関係数は 0.97 であり，FingerTPS が接触力を忠実に再現出来ていることが確認できる．

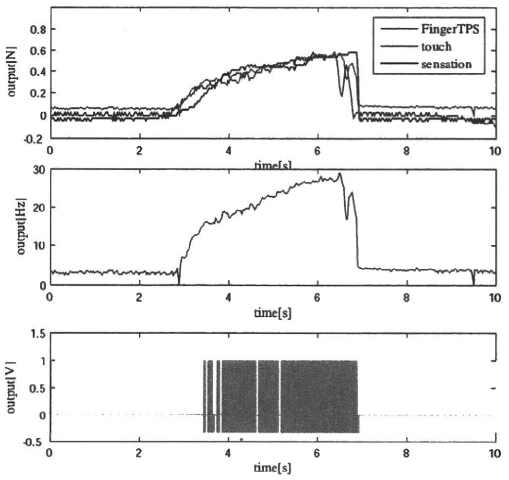

Fig.8 Response of subjective pressure sensation evoked by the microelectrical stimulation, pulse train for the microelectrical stimulation, and the actual force applied to the Finger TPS system,

4. 結言

触覚センサの出力をマイクロスティミュレーション法により神経フィードバックし，人工感覚を提示するシステムを構築した．触覚センサの出力をパルス変換し，マイクロスティミュレーション法により提示することで失われた感覚を補綴しうる可能性を示した．

文 献

[1] M.Shimojo,T.Suzuki,A.Namiki,T.Saito,M.Kunimoto, R.Makino,H.Ogawa,M.Ishikawa,K.Mabuchi "Development of a system for experiencing tactile sensation from a robot hand by electrically stimulating sensory nerve fiber" IEEE Trans.Robotics and Automation(CD-ROM),2003

[2] Kandel,Schwartz,Jessell"PRINCIPLES OF NUERAL SCIENCE Fourth Edition",McGraw-Hill,2000

[3] T.Suzuki,K.Mabuchi,H.Nishimura,T.Saito,N.Kakuta, M.Kunimoto,M.Shimojo,The Relationship between Stimulation Signals and Subjective Intensities and Areas, Proc. Int. Conf. of the IEEE EMBS,Atlanta, 459, Oct. 1999.

Linking human nervous system with mechanical control system of next-generation artificial organs

Kunihiko Mabuchi
Graduate School of Information Science and Technology, The University of Tokyo

１．はじめに

近年、生体の神経系と機械系の情報ラインを直接接続し、運動神経系の情報によって義肢などの外部機器を制御したり、逆に、求心性の感覚神経系に外部から刺激を入力する事によって、人為的に感覚を発生させたりする所謂ブレイン・マシン・インタフェース（ＢＭＩ）システム、或いはブレインコンピュータインタフェース（ＢＣＩ）システムとか呼ばれるシステムの開発が盛んに行われるようになってきているが、次世代の人工臓器や人工器官では、これらの技術を用いて生体の神経系と人工臓器・人工器官を直接結んだシステムを開発していく事が大きな目標となって来るであろうと思われる。

神経系には大別して遠心性の運動神経系・自律神経系と求心性の感覚神経系とがあるが、遠心性の神経系と外部機器を接続するいわゆる出力型のＢＭＩシステム(人工臓器)としては、運動神経系では、随意運動機能を持つ義肢が典型的な例であり、また、自律神経系に関しては、交感神経系の活動や副交感神経系の活動情報によって、最適な条件で作動する人工心臓システムなどがその例として挙げられる。

一方、求心性の感覚神経系と人工の感覚器（センサ)を接続する､いわゆる入力型ＢＭＩ(人工感覚器)に関しては、人工聴覚（人工内耳）は臨床的に最も成功しているＢＭＩシステムであり､すでに 30 年間の歴史と 10 万人以上の患者を持つ確立した治療法となっている。また、人工視覚もまだ実験段階ではあるが、多くの施設で研究が進められてきており、人を対象とした実験も行われつつある。

このような、所謂ブレイン・マシンインタフェースシステムの急速な発展は、近年における脳科学の進展や MEMS (micro-electromechanical system) 技術の進歩を背景としたものであるが､DARPA (米国の国防省国防高等研究計画庁) 等、軍事関係の組織が非常に大きな予算を投入してプロジェクトを推進して来た事も関与している。また、マスコミでは、いわゆる「光」の面を中心に取り上げる事もあり、あたかも（一般には）明日にでもこのような技術が実現するかのような印象が抱かれちであるが、人工臓器・人工器官の領域でＢＭＩシステムを実際の臨床に耐えうる段階まで進めるには、電極の開発やコーディング・デコーディング則の解析など、まだ多数の問題点が残っており、これからも長い期間と地道な努力が必要ではないかと考えている。

２．電極を中心とした諸問題点について

先に挙げた問題点の中で、最大のものは、神経系と機械系の間で情報の入出力をどのように行うかという手法の問題であり、これには、１）非侵襲的手法によるか、侵襲的手法によるか、２）情報の入出力を何処で行うか、などの側面がある。神経活動の非侵襲的計測法としては、現在、脳波 (EEG)、脳磁図 (MEG)、機能的 MRI (fMRI)、近赤外スペクトロスコピー (NIRS) などが試みられているが、得られる情報量や空間分解能､リアルタイム性に問題が有り、現在は精細な義手の運動制御や感覚生成を行おうとする場合には、主に金属ワイヤ電極や剣山型電極などを直接神経系に刺入し、計測・刺激を行う侵襲的方法が主流で、その他、開頭はするが、刺入は行わず、柔軟なシリコンなどで出来たシートに電極アレイを配置した所謂 ECo-G (皮質電図)電極を硬膜下に留置して低侵襲的に local field potential の計測や刺激を行う試みも多数行われている。

情報の入出力を行う部位としては、中枢神経系（脳）と末梢神経系があるが、極端にいえば、脳の機能が侵されずに残存していれば、同部位にアクセスする事によってほぼ全ての病態に対応する事が可能で、形態的にもアクセスしやすいため、大脳皮質が多く用いられるが、万が一、感染や組織の損傷などの合併症が発生した場合の危険性を考えると、末梢神経でのアクセスの方が有利な面もある。侵襲的手法で用いる電極に関しては、昔から用いられる金属ワイヤ電極や針電極をベースにしたもの、ＭＥＭＳ技術をベースにしたプローブ電極類、又、パリレンなどの柔軟な材料を用い、流路構造などを付加したものなど、多様な電極が開発されてきているが、チャンネル数や柔軟性や生体適合性を含めた材料の問題、インピーダンスの問題など、長期の安定した使用にはまだ多くの問題が残っている。又、末梢神経用の電極に関しては、以前から研究されている神経再生型電極などの他に、近年、LIFE(Longitudinal Intra-fascicular Electrode) や FINE(Flat Interface Nerve Electrode) などが考案･開発され、これらを用いた外部機器の制御も行われている。

紙面のスペースの関係で、神経信号のコーディング・デコーディング則の問題については、割愛したが､シンポジウムではこの点についても議論したい。

Key words: BMI, BCI, MEMS, electrode

32nd Annual International Conference of the IEEE EMBS
Buenos Aires, Argentina, August 31 - September 4, 2010

OPTIMIZING THE DIAMETER OF HOLES FOR FLEXIBLE REGENERATION MICROELECTRODE

Riho Gojo[1], Harukazu Saito[3], Takafumi Suzuki[2], Kunihiko Mabuchi[1,2]
[1]Dept. of Advanced Interdisciplinary Studies, Grad. School of Engineering, The University of Tokyo,
[2]Dept. of Information Physics & Computing, Grad. School of Info. Sci. & Tech., The University of Tokyo
and [3]National Hospital Organization Murayama Medical Center, JAPAN,

ABSTRACT

In this study, we suggest a new guideline for regeneration microelectrode to be implanted between the severed stumps of peripheral nerves, the microelectrode designed particularly for connecting the signal line of an artificial hand directly to the nerve system. The nerve regeneration microelectrode is an interface device expected to realize a BMI (brain-machine interface).

As the microelectrode device consists of a parylene cable and gold electrodes, it has good flexibility and biocompatibility. The advantage of this technique is that the electrode is in position to make continuous measurements throughout the regeneration process. On the tip of the device, holes are patterned with rounded gold electrodes, where a nerve fiber is growing and passing through each hole during regeneration. By using this unique technique, we can avoid damaging a nerve fiber and make to stable measurement in the long term.

We optimized the diameter of the holes located on the device. Furthermore, since the electrode is fully integrated into a nerve bunch, we can both stimulate the nerve cells by applying a voltage pulse to the motor nerve and take sensory nerve measurements. With this extent of control, we can also selectively measure the signals from these nerve fibers.

1. INTRODUCTION

When a peripheral nerve fiber is severed or badly damaged, the body begins to repair the damaged region between the two nerve stumps with different processes from specific directions. Initially, the end of the distal region begins a process called Wallerian degeneration where the end of the distal nerve begins to break down, while simultaneously forming a fibrinous bridge; this bridge is made from fibrin and eventually links the two nerve stumps. It is believed that axon growth is inhibited until this bridge reaches the proximal nerve stump. Once connected, by the bridge, axons begin to grow down along it towards the distal nerve stump [1].

Measuring the current from single nerve cells is extremely difficult due to the inability to isolate individual cells and because of the difference of the length-scale between the cells and the electrodes. However, a microfabricated electrode presents a unique opportunity to isolate individual nerve cells and measure current through them, as explained here: Each regenerating nerve cell must grow linearly to bridge the gap between the severed stumps during nerve fiber regeneration. Therefore, by placing a microfabricated electrode in the path of regenerating nerve cells, we can isolate individual cells and measure the current through them once the nerve fiber has healed. By placing a microfabricated electrode in the path of the regenerating nerve cells, we can isolate individual cells and measure the current through them once the nerve fiber has healed.

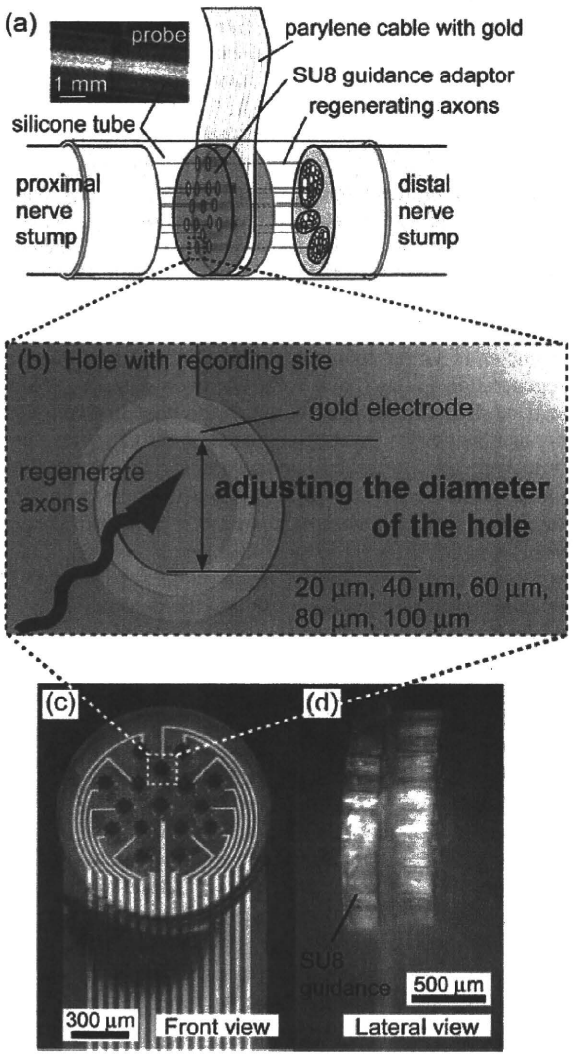

Figure 1: Schematic diagrams of the adjusting the diameter probe. (a) We designed a probe with 16 micrometer-sized holes in order to direct regenerating axons at a severed gap of stumps through the holes. (b) Hole at recording site for the regenerating axons, to selectively study cell growth by adjusting the hole diameter. (c-d) Photographs of the fabricated probe.

The advantage of this technique is that the electrode is in position to make continuous measurements throughout the regeneration process. Furthermore, since the electrode

is fully integrated into the nerve bunch, we can both stimulate the nerve cells by applying a voltage pulse and take long-term measurements.

The sieve enables nerve fibers to regenerate through metalized holes; these holes serve as the electrodes. However, since these sieve electrodes are 2D, they provide no guidance for nerve cells that reach a region of the electrode without holes. The cells simply grow randomly and find the holes by chance. In addition, since these electrodes and cables are made from hard materials such as silicon and glass [2-3] because the devices is bigger than the target nerve, the possibility that it may damage the surrounding tissue is high.

At IEEE MEMS 2009, we presented a technique to fabricate an electrode capable of simultaneously enabling current measurements and application of stimulation to nerve cells during and after nerve cell regeneration (Fig. 1) [4].

However, so far, no research has been conducted on determining a suitable hole diameter. We consider that the hole diameter affects the accuracy and sensitivity of measurement on the nerve regeneration process. If the hole diameter is larger than that of the nerve fiber, the nerve regeneration is quick and well; however, detecting a signal will be difficult because the electrode dose not completely contact the nerve. On the other hand, in the case of a smaller hole diameter, the nerve fiber may not pass through the holes. Once the nerve has grown and passed through the holes on the device, it will be possible to obtain signals from the nerve without noise. In order to determine a suitable hole diameter, we fabricated five devices, each with a particular hole diameter, and compared signal responses after the implantation of these devices.

Here, we suggest a new guideline for a regeneration microelectrode to be implanted between the severed stumps of axons.

2. DESIGN AND FABRICATION

Target nerve

We focus on the sciatic nerve in rats because it is a useful nerve to target as it controls the manner in which a rat walks. A normal rat walks on its toes; however, if the sciatic nerve is severed, it begins to walk flat-footed. Upon recovery of the sciatic nerve, it once again begins to walk normally. We can perform a walking track analysis of rats to evaluate the function of their peripheral sciatic nerve, [5] and as a result, we can confirm whether it has healed without operating.

Fabrication Process

Our flexible probe comprises a thin biocompatible polymer film (parylene) with 16 holes, within which we encase an electrode [6-7] (Fig. 2).

The fabrication procedure is as follows: We first pattern a gold layer on a thin parylene film (Fig. 2(a) and (b)). The thickness of the gold layer is 400 nm. Gold and parylene are patterned with a photoresist (S1818) by standard photolithography. Next, we deposit and pattern a second parylene film (Fig. 2(c–e)). Each parylene film is 20-μm thick. Peel off the electrode from the wafer (Fig. 2(j)). Finally, we complete the process by fabricating the guidance

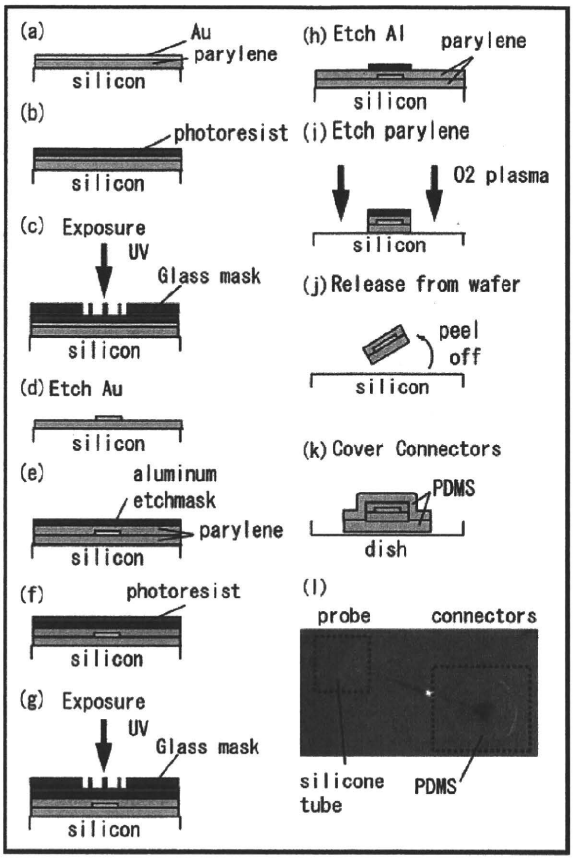

Figure 2: Schematic diagram of fabrication process. (a-b) First, a gold layer was patterned on a parylene film; then, (c-e) the second parylene film was deposited and patterned. (f-i) an electrode was fabricated with O_2 plasma, and (j) it was peeled off from the wafer. (k) Finally, the process is completed by fabricating the connectors with PDMS.

holes on the other side (Fig. 2(k-l)).

Selectivity through Probe Design

Five electrodes have been fabricated, each with a different hole diameter (20, 40, 60, 80, or 100 μm), so as to compare and optimize the hole size for stimulating and nerves and recording nerve signals; the nerves are typically 10 to 20 μm in diameter.

3. EXPERIMENTAL RESULTS

The sciatic nerve was cut and led into a silicone tube. Two months after the implant, afferent and motor signals were recorded. The signals recorded using devices with a hole diameter (Φ of 80 μm tended to be clear (Fig. 4), although a slight difference was found in afferent and motor signals. In addition, the signals recorded from the right hind leg were weaker than those recorded from the left hind leg.

Different levels of recovery of the function were observed depending on the diameter of the holes on the electrode section. Devices with a hole diameter larger than

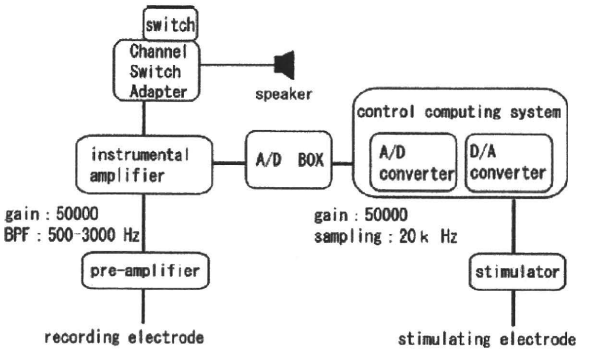

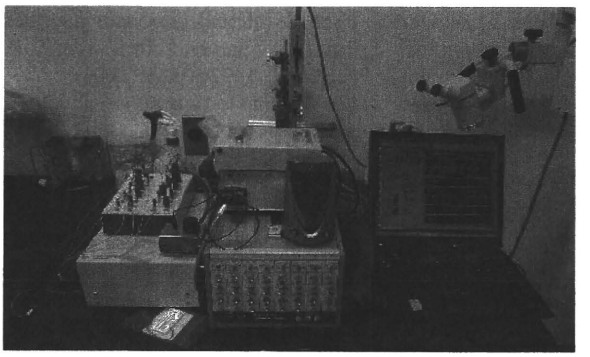

Figure 3 (a) Block diagram and (b) devices of the recording and stimulating system. Recording electrodes were connected to a computer via pre-amplifier, instrumentation amplifier, and A/D converter. Stimulating electrodes were also connected to the computer via D/A converter and stimulation device.

Φ60 μm seemed to produce a high level of recovery, while those with hole Φ20 μm led to only a small level of recovery. As showed in Fig. 5, ulcers formed on the toes of the

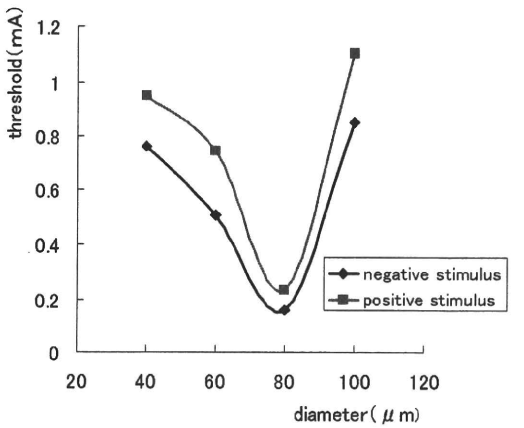

Figure 4: Minimum currents (threshold) to induce a stitch in a hind limb with various diameters of electrode holes.

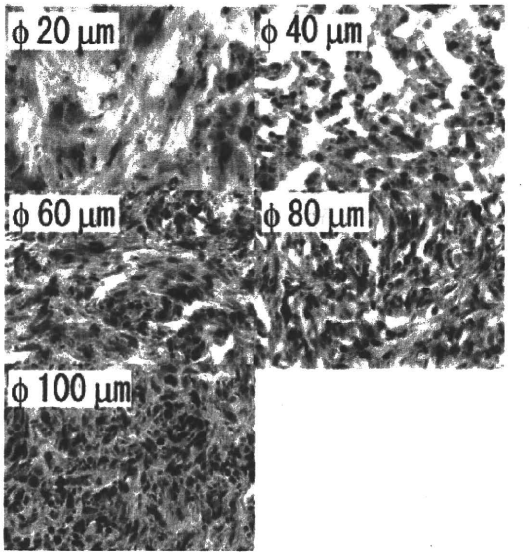

Figure 5: Pictures of hind limbs, recorded two months after the implants. Side view on the left and bottom view on the right. Arrows show ulcers formed on the skin.

stimulated legs when devices with holeΦ40–80 μm were used. This result may indicate that the rats had unusual perception owing to incomplete restoration of nerve fibers.

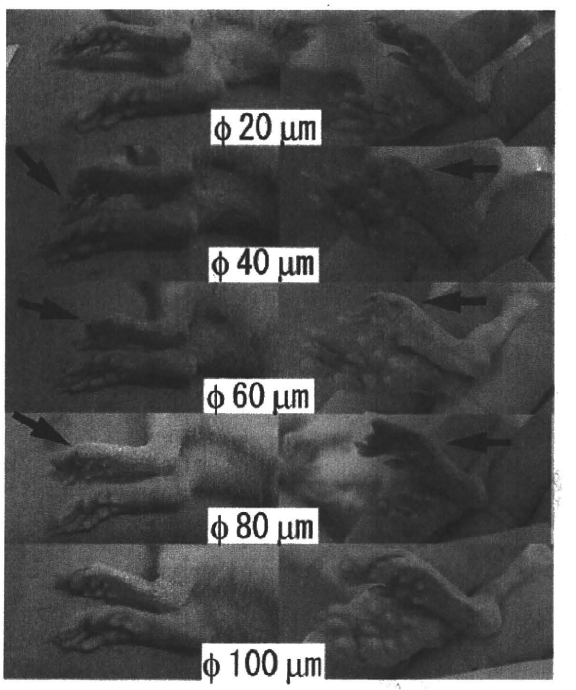

Figure 6: Images captured by phase-contrast microscopy. The proximal side of the electrode is sliced in the vertical direction. Red: anti-MBP antibody, Blue: antineurofilament antibody.

The sciatic nerves containing the electrodes were resected and were fixed by 4% paraformaldehyde and frozen sectioned (Fig. 6). The sections were stained with an antineurofilament antibody and an anti-MBP (myelin basic protein) antibody. The regeneration axons of Φ20 μm were few in the case of pigmentation with the antineurofilament antibody on the distal side of the electrode, and a large number of regeneration axons with Φ40 μm or more were admitted. Further, numerous parts

with comparatively large positivity and Φ40 μm or more were observed, though they lay scattered in small parts of Φ20 μm in the dye with the anti-MBP antibody. It was considered that the c with a large diameter and containing a marrow fiber had regenerated through the electrode and formed these parts of Φ40 μm or more.

We found that the threshold to induce a stitch in a limb depends on the diameter of holes on the microelectrode device (Fig. 4). The minimum value of the threshold was obtained to be 0.2 mA with a hole of Φ80 μm. We observed ulcers on the toe of the stimulated legs, particularly in the case of hole diameters ranging from Φ40 μm to Φ80 μm.

4. CONCLUSION

In summary, we propose a regeneration-type electrode that represents important advances over the present neural electrodes. By considering the overall results, we conclude that a hole diameter of 80 μm is suitable for facilitating nerve regeneration and performing sensitive measurement.

Our future plan is to integrate multiple electrodes having holes of a suitable size into this flexible device so as to perform multi-channel measurement.

REFERENCES

[1] Y.-C. Lo, *et al.*, Neural guidance by open-top SU-8 microfluidic channel, *IEEE MEMS*, Maastricht, January, pp. 671-674, 2004.

[2] W.L.C. Rutten, Selective electrical interfaces with the nervous system, *Annu. Rev. Biomed. Eng.*, vol. 4, pp. 407-452, 2002.

[3] T. Akin, *et al.*, A micromachined silicon sieve electrode for nerve regeneration applications. *IEEE Trans. on BME.*, vol. 41, pp. 305-313, 1994.

[3] R. Gojo, *et al.*, A flexible regeneration microelectrode with CELL-GROWTH GUIDANCES, *IEEE MEMS*, Sorrento, January, pp. 256-259, 2009.

[4] T. Suzuki, *et al.*, Flexible microelectrode for interfacing regenerating peripheral nerves, Proc. of 19th International *IEEE EMBS.*, 1997 (CD-ROM).

[5] G. M. T. Hare, *et al.*, Walking track analysis: a long-term assessment of peripheral nerve recovery. *Plast Reconstr Surg*, vol. 89, pp. 251-258, 1992.

[6] T. Suzuki, *et al.*, Flexible microelectrode for interfacing regenerating peripheral nerves, Proc. of 19th International *IEEE EMBS.*, 1997 (CD-ROM).

[7] S. Takeuchi, *et al.*, 3D Flexible multichannel neural probe array, *Journal of Micromechanics and Microengineering*, vol. 14, pp. 104-108, 2004.

32nd Annual International Conference of the IEEE EMBS
Buenos Aires, Argentina, August 31 - September 4, 2010

RatCar: A vehicular neuro-robotic platform for a rat with a sustaining structure of the rat body under the vehicle

Osamu Fukayama, *Member, IEEE*, Takafumi Suzuki, *Member, IEEE*, and Kunihiko Mabuchi, *Member, IEEE*

***Abstract*— An online neuro-robotic platform in the form of a small vehicle, the "RatCar" has been developed. First, a rat had neural electrodes implanted in the motor cortices to record extracellular potentials. Then, our system combined the rat and its vehicle body by hanging the rat under its floor. In this paper, an experimental platform is proposed to observe and analyze motor commands by correlating neural signals with locomotion states. It was designed to operate in 2 modes; (a) adaptively correlating neural signals and locomotion states to determine motor commands, and (b) applying the estimated motor commands to control the vehicle according to the intention of the rat. As a result, time-varying correlation between neural and locomotion activities has been adaptively visualized in real time to analyze motor commands in various body conditions. In addition, a control of the vehicle has been improved.**

I. INTRODUCTION

Brain-machine interfaces (BMIs) are currently of interest because of their ability to provide a new modality for devices control. While a number of applications are already tested on human beings using non-invasive measurement of brain activity such as the electroencephalogram (EEG), direct recording of the extracellular potentials is a promising technique to extract motor commands to control artificial devices more precisely. Chapin et al [1], for example, developed a system to control the movement of a robotic arm using the neural signals from the primary motor cortex of a rat. More complex control of a robot arm through the neural signals of monkeys were reported by Wessberg et al. [2].

Our BMI system is in the form of a small vehicle, which we call the "RatCar". It is unique in that a neural signal source (i.e., a rat) is integrated inside the device (i.e., the vehicle body) and the whole components move around. The rat is therefore provided with direct visual and sensory feedback as the vehicle moves. We expect that this condition enables the rat's brain to modify itself adapting to the vehicle system. Our ultimate goal is to let the vehicle collaborate with the brain to achieve a locomotion as the rat intended on behalf of natural limbs.

A rough estimation of the locomotion according to neural signals had been achieved in the past study by the authors [3] to determine the movement of the vehicle. In this paper, the vehicle form was revised by elevating the floor higher to hang a rat under the vehicle body. Its shape placed a rat closer to the ground so that it was capable of exploring the ground freely. It also enabled a "passive" control mode of the vehicle. In this mode, the vehicle was neutralized by detaching motors, and a rat was trained to tow the vehicle. Correlation parameters representing motor commands were compared in various situations.

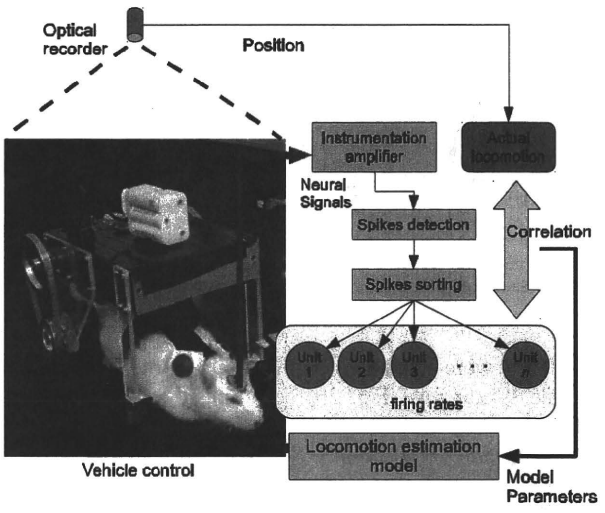

Fig. 1. Block diagram of the RatCar system. The vehicle to move around on a field holding a rat, recorders for neural signals and locomotion states, and a locomotion estimation model to determine vehicle movements are connected.

II. METHODOLOGY

Our system consists of the vehicle to move around on an experimental field (2 m × 1 m), simultaneous recorders for neural signals and locomotion states, and a locomotion estimation model which correlates those two acquired values in real time to determine vehicle movements (Fig. 1).

A. Neural Signals Recorder

1) Implant: Neural electrodes have been fabricated with MEMS technology to acquire extracellular multiunit activities (MUA). Each electrode had 4 gold recording sites on a thin soft layer made of parylene polymers (Fig. 2a). Then, a small connector (1 mm - pitch IC socket) was attached to connect the lines to an amplifier.

This work was supported by Grant-in-Aid for Scientific Research (Y-Startup) 30508205 and (A) 20246045 from the Ministry of Education, Culture, Sports, Science and Technology of Japan and by Grant-in-Aid for Research on Advanced Medical Technology H17-Nano-010 from the Ministry of Health, Labour and Welfare of Japan.

All the experiments we performed followed guidelines given by the "Animal Experiments Committee of the University of Tokyo".

The authors are with Graduate School of Information Science and Technology, The University of Tokyo, 7-3-1 Hongo, Bunkyo, Tokyo, JAPAN of@ratcar.org

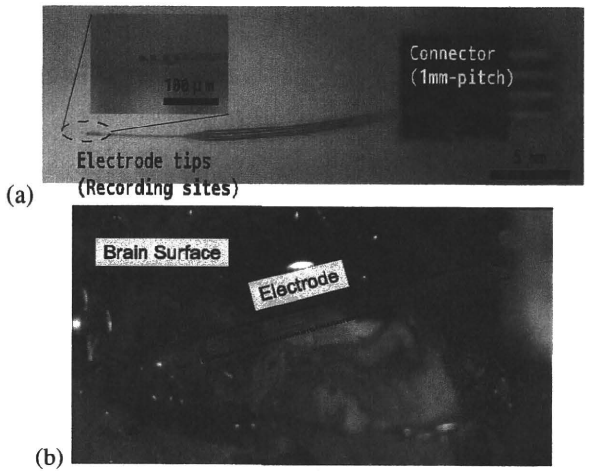

Fig. 2. (a) A fabricated electrode which has 4 recording sites on a tip and a connector on the other end. (b) Electrodes implanted in the brain penetrating the surface. Dura mater had been removed in advance.

They were implanted in the motor cortical regions of 8 male Wistar rats (Fig. 2b) according to a stereotaxic atlas [4] and functional localization maps [5], [6].

2) Signal Acquisition: Neural signals were derived by differentiating potentials between 3 recording sites and 1 reference site on each electrode. They were then amplified and filtered (Gain: 5,000, BPF: 500 - 5,000 Hz) by *Multichannel Systems PGA-64* or *FA-64* followed by an A/D converter (*National Instruments PCI-6071E*, 20 kSps for each channel) installed in a personal computer.

3) Spikes Detection and Sorting: Neural firing sequences $\vec{s}_t$ were detected as the recorded waveform showed local maximal or minimal values. Note that either positive or negative peak were counted as neural firings because of the differential recording setup.

Then, a Gaussian-mixture model (GMM) sorted the distribution of detected spikes z_t into classes representing n-th neuron ($n = 1, \ldots, N$) respectively. Each neuron were assumed to generate spikes with a constant peak amplitude μ_n distributed by a Gaussian $N(\mu_n, \sigma_n^2)$ (μ_n: mean, σ_n^2: variance). Consequently, the distribution of peak amplitudes $P(z)$ were described as

$$P(z) = w_n N(z;\, \mu_n, \sigma_n^2), \tag{1}$$

where w_n is a prior probability of each Gaussian.

The expectation-maximization (EM) algorithm[7] estimated the parameters w_n, μ_n, σ_n^2 for the GMM while a number of Gaussians were determined by searching maximum likelihood of GMM as increasing the number. Finally, a class n to give a maximum probability $P(z|n)$ to generate a spike z_t were chosen.

B. Locomotion Recorder

An optical position tracker (*KEYENCE CV-5700*) was installed over the experimental field. The system captured an image in 1024 × 768 resolution every 100 ms to detect positions of 4 colored markers. While 2 markers were placed on the back of each rat (Fig. 3), the other 2 markers were placed on the vehicle. Velocity (Fig. 4(a)) and directions of the rat and the vehicle were calculated according to temporal changes and relative positions (Fig. 4(b)) of those markers.

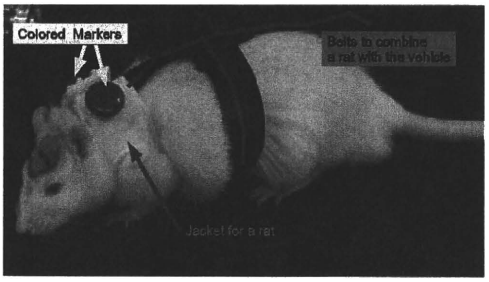

Fig. 3. A rat with markers placed on the back. A white jacket and a black belt was used to combine the rat with the vehicle.

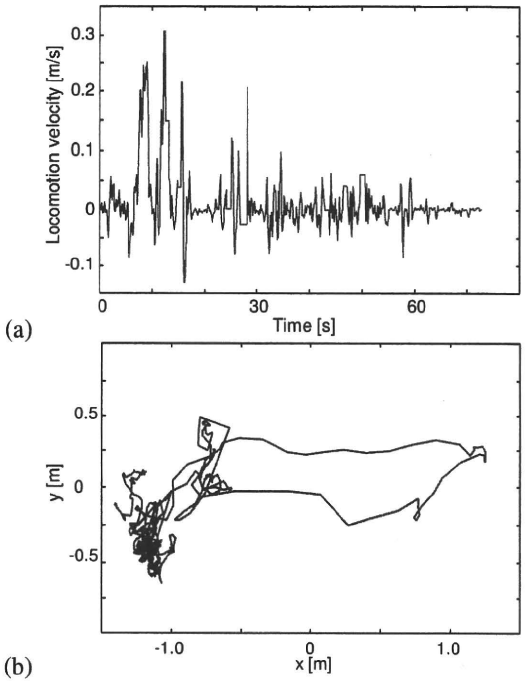

Fig. 4. An example of (a) locomotion velocity and (b) trajectory of a rat recorded with the optical position tracker.

C. Locomotion Estimation

1) Correlation Model: A state space model as described in equation (2),(3) correlated the neural firing rates $\vec{y}(p)$ and a locomotion states $\vec{x}(p) = (x_{\text{velocity}}(p),\ x_{\text{azimuthal variation}}(p))^{\mathrm{T}}$ (a velocity and azimuthal variation) at p-th bin every 100 ms;

$$\vec{x}(p+1) = F\vec{x}(p) + \vec{\xi}(p) \tag{2}$$

$$\vec{y}(p) = H_p\vec{x}(p) + \vec{\eta}(p) \tag{3}$$

where the state transition matrix F and output matrix H_0 were initially tuned for each subject in the first trial so that the estimation result or vehicle should not go out of control.

Here, the Kalman filter algorithm were applied to the model to estimate the locomotion states $\hat{\vec{x}}(p)$ by sequentially acquired neural firing rates $\vec{y}(p)$:

$$\hat{\vec{x}}(p+1) = F(I - K_p H_p)\hat{\vec{x}}(p) + FK_p\vec{y}(p). \quad (4)$$
$$(K_p : \text{Kalman gain})$$

2) Online Update of Parameters: Meanwhile, an observation update algorithm of the Kalman filter are capable of updating the output matrix H when an actual locomotion states were provided as a teaching source.

Assuming the neural firings sequence were orthogonal, the H were decomposed to the elements corresponding to each neuron n (i.e., $H = (\vec{h}_{n,p}) = (h_{n1,p}, h_{n2,p})$) and they were updated individually:

$$\hat{\vec{h}}_{n,p+1} = (I - K_{n,p}\vec{x})\hat{\vec{h}}_{n,p} + K_{n,p}\vec{y}(p). \quad (5)$$
$$(K_{n,p} : \text{Kalman gain for each neuron } n)$$

D. Vehicular Body and Control

According to the estimated locomotion velocity and azimuthal variance, the vehicle which had a high-floored structure hanging a rat under the floor was controlled to trace the actual movement of the rat. The control operated in 2 modes; a "passive" mode and a "neuro-robotic" mode. In the passive mode, the motor driver of the vehicle was neutralized and the rat was loosely binded to the vehicle body towing it. In the neuro-robotic mode, the rat was sustained under the vehicle floor by the jacket and belt (Fig. 3) so that its limbs gently touched the ground.

In this paper, those modes were applied to compare neural activities in 3 situations; natural locomotion (by the own limbs of a rat), half-robotic locomotion (passive mode; a rat towed the vehicle), and full-robotic locomotion (neuro-robotic control of the vehicle hanging a rat).

III. RESULTS AND DISCUSSION

A. Parameters Update

In an initial period of each trial, a rat was left on the field and freely moved around. The correlation parameters that we initialized with 0.0 were updated, and they converged in less than 40 seconds on most trials. A typical result is shown in Figure 5(a).

Then, the rat was binded with the vehicle and motivated to move by an experimenter blowing on its back. As a result, the parameters showed remarkable changes as the rat started moving with the vehicle, then they fell into another converged states (Fig. 5(b)).

Finally, the rat was moved by the vehicle in the neuro-robotic mode. In this situation, the parameters were updated using the correlation between neural firings and actual movement of the vehicle. The parameters should be kept converged if the estimation of the vehicle control had been proper. Those results were observed widely on any rats although the converged values was different for each subject.

The fact that the parameters converged in 40 seconds during the free locomotion suggests that our simple model

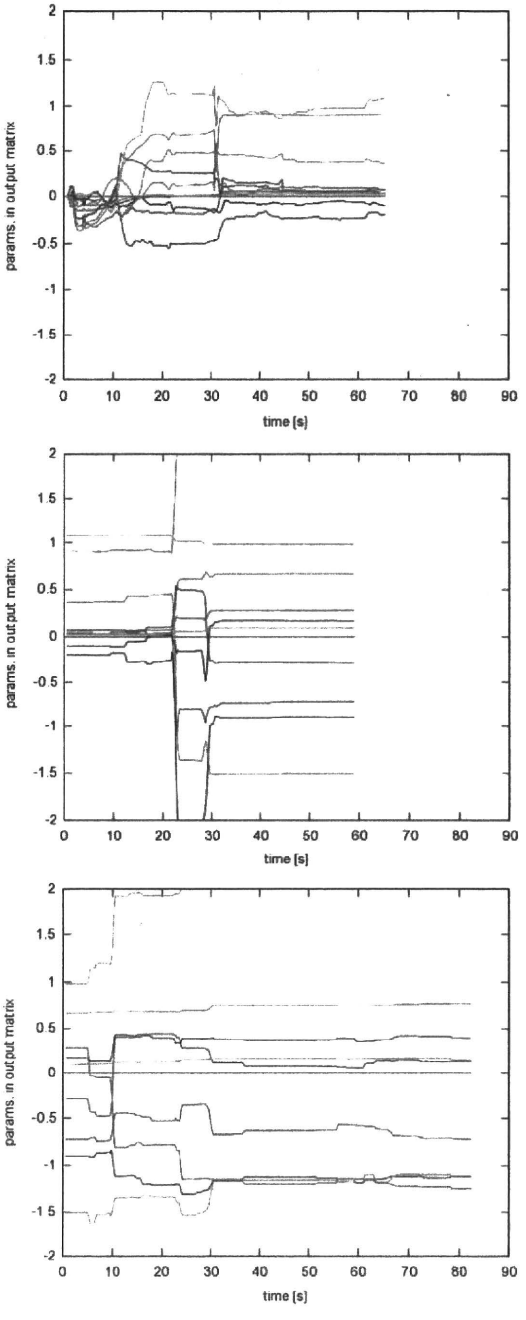

Fig. 5. Adaptively updated correlation parameters (elements of output matrix H) observed (a) as a rat freely moved on the field in an initial identification period, (b) as a rat towed the vehicle, (c) as a rat was moved by the vehicle in neuro-robotic mode.

were applicable to describe motor commands. Then, as the rat was binded with the vehicle, the most parameters increased. It is reasonable because the rat brain should send stronger motor commands to muscles to move the vehicle and its original body as a whole.

However, neuro-robotic control of the vehicle resulted in sudden variation of the identified parameters which should be unchanged if a proper motor commands representation was realized by our model. Some pairs of 2 parameters were passing each other (typically on 10 seconds from the start point in Fig. 5(c)), which may suggest an improper spike sorting.

B. Vehicle-Rat Integration

The system was capable of holding a rat under the vehicle floor, and the rat looked relaxed as long as the vehicle was neutralized (in passive mode). Weight of the whole vehicle was less than 1 kg and a rat (varied from 300 g to 500 g in weights) was able to tow the vehicle on a flat field.

In the neuro-robotic mode, the motors which were sealed inside the body succeeded in not making the rats frightened as the vehicle gently moved. Most rats (6 out of 8) were tamely hanged under the vehicle, although 2 of them became hyperactive to turn down the whole system.

C. Future Direction

Another problem with our current system is that we cannot compare an estimated movement of the vehicle to real intention of a rat in neuro-robotic mode, because the rat was forcibly moved with the vehicle even if it tried to move to other direction. A force measurement device should be attached to the belt binding a rat body and the vehicle so that the motion errors between those two are measured.

IV. CONCLUSION

In this paper, a neuro-robotic platform has been proposed to observe and analyze motor commands by comparing correlation between neural signals and locomotion states in various situations. It is capable of applying other electrodes or motor decoders to find out a better methods to realize precise brain-machine interfaces.

REFERENCES

[1] J. K. Chapin, K. A. Moxon, R. S. Markowitz, and M. A. Nicolelis, "Real-time control of a robot arm using simultaneously recorded neurons in the motor cortex," *Nature Neuroscience*, vol. 2, no. 7, pp. 664 – 670, 1999.

[2] J. Wessberg, C. R. Stambaugh, J. D. Kralik, P. D. Beck, M. Lauback, J. K. Chapin, J. Kim, S. J. Biggs, M. A. Srinivasan, M. A. L. Nicolelis, "Real-time prediction of hand trajectory by ensembles of cortical neurons in primates," *Nature*, vol. 408, pp. 361 – 365, 2000.

[3] O. Fukayama, N. Taniguchi, T. Suzuki, K. Mabuchi, "RatCar System for Estimating Locomotion States using Neural Signals with Parameter Monitoring: Vehicle-formed Brain-Machine Interfaces for Rat," *Proc. 30th Annual International IEEE EMBS Conference*, pp. 5322 – 5325, 2008.

[4] G. Paxinos and C. Watson, The Rat Brain in Stereotaxic Coordinates, Compact Third Edition. Academic Press, 1997.

[5] R. D. Hall and E. P. Lindholm, "Organization of Motor and Somatosensory Neocortex in the Albino Rat," *Brain Research*, vol. 66, pp. 22 - 38, 1974.

[6] S. P. Wise and J. P. Donoghue, Motor cortex of rodents. *Motor Cortex*, Plenum Press, 1984.

[7] A. P. Dempster, N. M. Laird, D. B. Rubin, "Maximum Likelihood from Incomplete Data via the EM Algorithm," *J. R. Stat. Soc. Ser. B*, vol. 39, no. 1, pp. 1 – 38, 1977.

32nd Annual International Conference of the IEEE EMBS
Buenos Aires, Argentina, August 31 - September 4, 2010

Estimation of finger postures to control a maniform device for playing a trumpet using electromyographic signals with external triggers

Yutaro Kobayashi, Osamu Fukayama, Takafumi Suzuki, and Kunihiko Mabuchi

***Abstract*—Electromyographic (EMG) signals have been used to control active prosthetic arms for amputees. One of the obstacles in making such prosthetic arms is the *timed estimation of posture*, because EMG signals and muscle movements are not necessarily synchronized. We estimated the finger motions for trumpet players by using both surface EMG (sEMG) and the timing information using body motion. The algorithms consisted of Principal Component Analysis (PCA), and Support Vector Machine (SVM). The results showed that applying the timing information using body motion increases how precisely the motion of the fingers is estimated.**

I. Introduction

Electromyographic (EMG) signals have been used to control active prosthetic arms for amputees. One of the obstacles in creating such prosthetic arms is the *timed estimation of posture* because EMG signals and muscle movements are not necessarily synchronized (Fig. 1(a)). Therefore, the precision of posture estimation can be significantly improved by externally providing timing information using body motion. An experimental system for playing the trumpet with surface EMG (sEMG) signals to show the validity of our claim has been developed and shown as Fig. 1(b). The system recorded sEMG signals from the forearm muscles of trumpet players. The postures of the hands that push the trumpet valves were estimated using the sEMG signals while the correct timing in which the valves were pushed was externally provided.

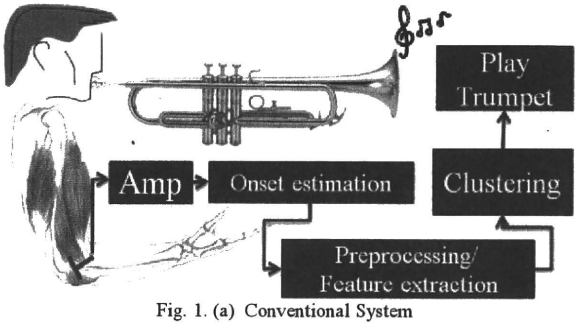

Fig. 1. (a) Conventional System

Manuscript received April 23, 2010.

Y. Kobayashi, O. Fukayama, T. Suzuki, and K. Mabuchi are with Graduate School of Information Science and Technology, the University of Tokyo, Tokyo, Japan(phone: 81-3-5841-6880;
e-mail: Yutaro_Kobayashi@ipc.i.u-tokyo.ac.jp).

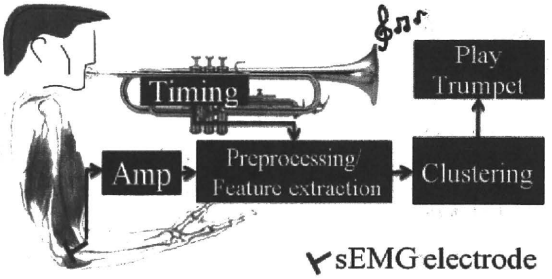

Fig. 1. (b) Proposed System

A. Motor Neurons and Muscles

Brains transmit motion orders to axons of upper motor neurons inside brains, and then to spinal cords. These orders are then transmitted through the synapses of lower motor neurons. Axons of the lower motor neurons become peripheral nerves and make synapses with muscle fibers. All the corresponding muscle fibers that a single motor neuron innervates are called the *motor unit*. There are over 1000 muscles controlled by a single motor neuron. When the orders reach the muscles, the muscles contract and the EMG signal is recorded.

B. EMG and Motor Unit Recruitment

Motor unit recruitment is defined as "the successive activation of the same and additional motor units with increasing strength of voluntary muscle contraction" [1]. Muscles use the recruitment process to generate various types of forces. The central nervous system increases the strength of muscle contractions by the following steps.

(A) Increase the number of motor units

(B) Increase the firing rate of each motor unit

At lower levels of muscle contraction strength, step (A) is prominent. However at the same time, step (B) is also observed which explains the complexity of motor recruitment.

There is also a recruitment sequence for different types of motor units: S(Slow), FR(Fast, Resistant), and FF(Fast, Fatigable) are the three main types of motor units and are recruited in the sequence of S, FR, and FF. Addition to the recruitment sequence, larger muscle contraction strength is generated by increasing the firing rate of motor units. Even if the subject makes a specific motion, the muscles near the target areas of the electrodes may only generate a feeble sEMG signal. This causes the difficulty in detecting the *onset* timing when dealing with sEMG signals[2][3].

C. General Characteristics for Playing the Trumpet

Trumpet players make different pitches by pushing the 3 valves in different patterns with the right hand. The 2nd finger controls the 1st valve (the valve closest to the mouthpiece), and the 3rd and 4th finger control the 2nd and 3rd valve respectively. There are 6 patterns in which the valves can be pushed and are musical are shown in Figure 2. Surface EMG signals were recorded to estimate the postures of the three fingers. The correct timing in which the valves were pushed was also recorded (timing is given externally).

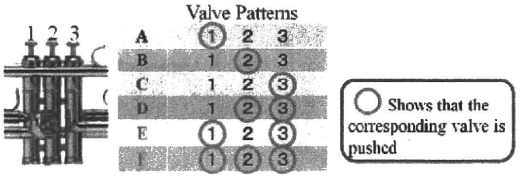

Fig. 2. Patterns of pushing trumpet valves

II. METHODS

A. Onset Detection Method

The selected threshold-based onset detection method [3], proposed by *Hodges and Bui*, has the characteristics for high onset detection rate and can be used for high onset detection. This method is used to estimate the timings of the valves pushed from sEMG signals. Equation 1 – 3 show how the onset is detected.

Here $\overline{v}_0$ shows the average of the first M data, $\overline{\sigma}_o$ shows the standard deviation of the first M (200) data, W shows the moving average of 5000 data, M shows the number of data used to calculate $\overline{\sigma}_o$, $\overline{v}_0$, t_a represents the estimated onset time, and h show the threshold (2.5).

$$t_a = \min\{k \geq W : g_k \geq h\} \tag{1}$$

$$g_k = \frac{1}{\overline{\sigma}_o}(\tilde{y}_k - \overline{v}_0) \tag{2}$$

$$\tilde{y}_k = \frac{1}{W}\sum_{i=k-W+1}^{k} y_k \tag{3}$$

The results were then used to compare with the actual valve pushed timings in section VI A, B.

B. Timing Information Provided Externally

The valve pushed timings were measured in two different methods. The first method measured the valve pushed timings by placing sensors onto the valves. The second method measured the timings of the breath by placing a vibration sensor onto the mouthpiece. In this experiment, the results of the first method were used as *timing information provided externally* for the simplicity.

C. Feature Extraction and Electrode Placement

Eight sEMG electrodes were applied to the subjects' right forearms (Fig. 3), and recorded with the sampling rate of 25 kHz. We extracted 0.16 second of data, right before the valves were pushed, was extracted. Covariance matrices were then calculated and used as features.

Electrode CH1 and 2 were placed on the extensor digitorum muscle to measure the flexion of all fingers. Electrode CH3 was placed on the flexor carpi radialis muscle to measure wrist movement. Electrode CH4 was placed on extensor indicis to detect the movement of the 4th finger. Electrode CH5 and 8 were placed on flexor carpi ulnaris muscle to detect the movement of the 4th finger. Electrode CH6 and 7 were placed on flexor digitorum superficialis muscle to detect the movement of 2nd and 3rd fingers respectively.

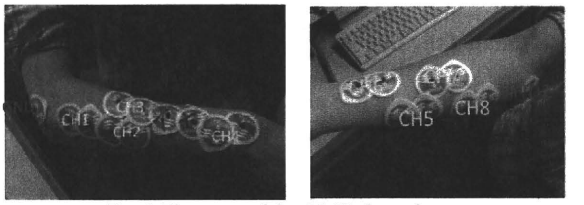

Fig. 3. Placement of the sEMG electrodes

III. EXPERIMENT

A. Experiment I

Two subjects were asked to push the valves with the instructions of the following subsets.

(a) Push 1st valve *10 times (valve pattern A)
(b) Push 2nd valve *10 times (valve pattern B)
(c) Push 3rd valve *10 times (valve pattern C)
(d) Push 2nd, and 3rd valves *10 times (valve pattern D)
(e) Push 1st, and 3rd valves *10 times(valve pattern E)
(f) Push 1st,2nd, and 3rd valves *10 times (valve pattern F)

B. Experiment II

Two subjects (K, Y) were asked to push the valves with the instructions of the following subsets. Note that only valve patterns A, B, C have been conducted by the subjects.

(a) Push 1st valve *30 times (valve pattern A)
(b) Push 2nd valve *30 times (valve pattern B)
(c) Push 3rd valve *30 times (valve pattern C)
(d) Push 2nd, and 3rd valves *30 times (valve pattern D)
(e) Push 1st, and 3rd valves *30 times(valve pattern E)
(f) Push 1st,2nd, and 3rd valves *30 times (valve pattern F)
(g) Push 1st, 2nd, 3rd valve 10 times each in this sequence
(h) Push 1st, 2nd, 3rd valve randomly for 30 times
(i) Push all patterns randomly for 50 times

IV. RESULTS

A. Precision of Onset Detection Methods

The selected threshold-based onset detection method [3] was used to estimate the timings needed to push the valves from the 8 sEMG signal of each of the electrodes. The estimated number of times that valves were pushed (estimated number of times pushed) is shown in Figure 3. The bar lines shows the estimated maximum and the minimum number of times pushed through out Experiment I.

The results show that the *selected threshold- based onset detection method* was effective for CH 1, 2, and 3, which estimated the average number of times pushed around 7. However for CH4 and 6, the estimated average number of times pushed was around 2.

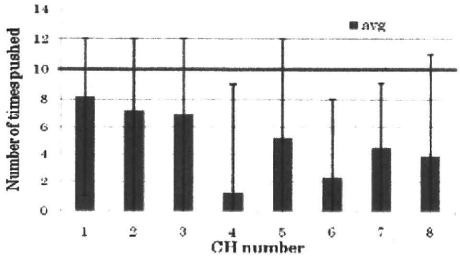

Fig. 4. Estimated number of times that valves were pushed by *selected threshold-based onset detection method for each CH*

To estimate the timings, CH1, which contained the best results for estimating the number of times that the valves were pushed, was selected. The estimation was conducted for subsets a, b, and c.

B. Use of Onset Detection Methods and Timing Information by Body Motion to Estimate Motion of Fingers

The features of the sEMG signals from one of the subjects were investigated by principal component analysis (PCA). The subsets of experiment I were limited to subsets a, b, and c in order to keep the analysis simple. The results analyzed using the timings provided externally are shown in Fig. 2(left), and. the results of the same subject analyzed using the timings estimated by *selected threshold- based onset detection method* are shown in Fig. 2(right). The patterns of the valves are classified much better in Fig. 2(left) than in Fig. 2(right).

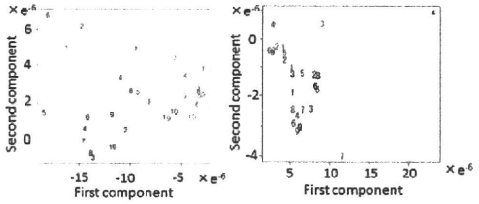

Fig. 5. PCA (left: timing is provided externally, right: onset detection method) *Numerical values show the order in which the valves were pushed in each valve pattern.
*Colors of the numerical values show valve patterns
(1st valve only: black; 2nd valve only: red; 3rd valve only: green)

C. Principal Component Analysis for Experiment II

Features of the sEMG signals from Experiment II were investigated by using principal component analysis (PCA). The PCA results (left: subject K, right: subject Y) for subsets a, b, c, and e are shown in Figure 6. As shown in Figure6 (left) shows that, the classification of the 1st and 2nd valve was not executed well for subject K, while Figure 6 (right) shows that, the 1st and 2nd valves were not well classified for subject Y.

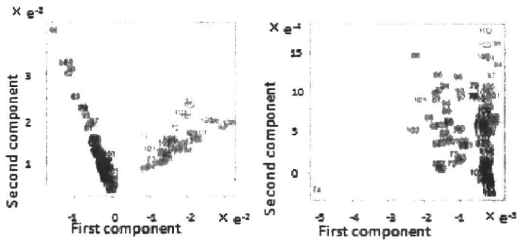

Fig. 6. PCA results for a, b, c, and e of Experiment II
(Left is subject A, and right: is subject B) *Numerical values show order in which the valves were pushed in each valve pattern.
*Colors of numerical values show valve patterns
(1st valve only: black; 2nd valve only; red, 3rd valve only: green)

D. Support Vector Machine

The same features used for the PCA were used for Support Vector Machine (SVM) analysis. Subsets a ~f from Experiment II were used as a training data set, and used to estimate the valve patterns for subsets d and e. Two kernel types, *linear*, and *Gaussian*, were used. The results of the estimation done by SVM are shown in Table I,II, and III.

TABLE I
ACCURACY OF SVM ESTIMATION FOR SUBJECT K

	Subject K					
Subset	g		h		i	
Kernel	radial	linear	radial	linear	radial	linear
A	80%	20%	50%	80%	73%	64%
B	100%	100%	100%	100%	100%	100%
C	80%	60%	73%	82%	0%	0%
D					60%	70%
E					100%	100%
F					17%	17%
Total	87%	60%	72%	86%	57%	57%

TABLE II
ACCURACY OF SVM ESTIMATION FOR SUBJECT Y

	Subject Y					
Subset	g		h		i	
Kernel	radial	linear	radial	linear	radial	linear
A	90%	90%	100%	60%	88%	50%
B	100%	100%	100%	100%	100%	100%
C	100%	100%	100%	100%	67%	83%
D					60%	20%
E					80%	60%
F					0%	40%
Total	97%	97%	100%	87%	73%	65%

TABLE III
ACCURACY OF SVM ESTIMATION FOR SUBECT K AND Y

	Subject K	Subject Y	Average
Linear kernel	66%	81%	73%
Radial kernel	70%	88%	79%
Average	68%	85%	76%

V. DISCUSSION

Selected threshold-based onset detection method [3] was used to estimate the valve pushed timings and Fig. 4 shows the estimated number of times that valves were pushed. Since each subset in experiment I had 10 trials, the ideal estimation results should be 10. However, number of times pushed varied depending upon electrode channels. These results show that precision of the method relies on selection of the right threshold, which requires further mathematical algorithm.

We selected CH1, which contained the best results for estimating the number of times that the valves were pushed, and used to obtain Fig.5 (right). Timing information provided externally was used to obtain Fig. 5 (left).

Each color on Fig. 5 represents the same valve pattern, therefore it is idealistic to be able to observe the same color in the same region. In Fig. 5 (left), all three patterns were located in distinct regions. On the other hand, in Fig. 5 (right), all three colors were assembled in disorder. These results suggest that externally providing timing information improves the precision of the estimation.

We conducted Experiment II to show the effectiveness of our proposed method, externally providing timing information using body motion. For both kernels, estimation for subject Y, a non-trained trumpet player, was 15% to 18% better than that of subject K, an experienced trumpet player. Our finding that the average estimation ratio of a non-trained trumpet player was better than that of a trained trumpet player when the hand postures were estimated using SVM, is attributed to the differences in their trumpet-playing ability. The non-trained trumpet player likely presented more overt characteristics for each of the valve patterns since his motions also included unnecessary movements. This strengthened the feature characteristics and enhanced the estimation precision of SVM.

VI. CONCLUSION

We showed that applying the timing information externally enables the motion of the finger to be estimated more accurately with the system developed. Also, we classified the valve patterns using two different types of kernels, and accurately distinguished all 6 valve patterns for playing the trumpet.

For future work, we plan to use timings from mouthpiece vibration as external triggers to estimate the valve patterns, and play the trumpet using the robot hand shown in Fig. 7.

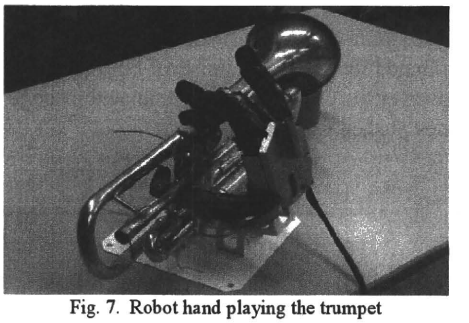

Fig. 7. Robot hand playing the trumpet

REFERENCES

[1] American Association of Electrodiagnostic Medicine. Glossary of terms in electrodiagnostic medicine. Muscle Nerve. 2001;Suppl 10:S1-50.

[2] M. Zecca et al.: "Control of Multifunctional Prosthetic Hands by Processing the Electro myographic Signal," Critical Reviews in Biomedical Engineering, pp.459−485 , 2002

[3] G. Staude et al.: "Onset Detection in surface electro myographic signals," Proc. Journal on Applied Signal Processing, Volume2, pp.67 −81, 2001

32nd Annual International Conference of the IEEE EMBS
Buenos Aires, Argentina, August 31 - September 4, 2010

Effect of simultaneous vibrations to two tendons on velocity of the induced illusory movement

Hiroaki Yaguchi, Osamu Fukayama, *Member, IEEE*, Takafumi Suzuki, *Member, IEEE*, Kunihiko Mabuchi, *Member, IEEE*

***Abstract*— A typical prosthetic limb has sensory shortcomings, one of which is lack of kinesthesia. Conventional methods to evoke kinesthesia, which would be required for a precise control of prosthetic limbs, include tendon vibration and skin stretch, but these produce only the sensation of small movements. In this study, tendon vibration is extended to evoke sensations of a more rapid movement. A stimulation method in which vibration is applied to two tendons is proposed, in contrast to most studies in which a single tendon was vibrated. Experimental results indicated that vibration applied to both ends of a muscle produces sensations of more rapid movement than vibration to just one. However, no significant difference in sensation was found between vibrating tendons of synergistic muscles and a single tendon.**

I. Introduction

RECENT research has improved the functions of prosthetic limbs. However, most of these limbs do not provide a kinesthetic feedback. Strong efforts have been made to provide humans with kinesthetic and other somatosensory information [1], [2], but such information cannot approach the abundance and accuracy of human sensory systems. Kinesthesia provides feedback signals to the human motor system, and therefore, prosthetic limbs would require appropriate kinesthetic feedback for a precise control.

Group Ia muscle spindle afferents and some types of cutaneous mechanoreceptors are the main sources of kinesthetic information. Transcutaneous vibration to a tendon [3]-[6] (Fig. 1), which activates Ia afferents, and skin stretch near the joint[7], [8], which activates the cutaneous mechanoreceptors, together can induce a kinesthetic illusion in a non-invasive manner. However, these stimulation methods produce only sensations of small joint movements (e.g. [5], [6], [9]). That is, the resultant angular velocity was about 5-10 deg/s, while human joints generally required to rotate in tens deg/s. In this study, tendon vibration has been extended to evoke a sensation of a more rapid movement. We have narrowed our focus to elbow extension.

Macefield et al. [10] reported that microstimulation to a single Ia afferent fiber generally failed to evoke kinesthesia.

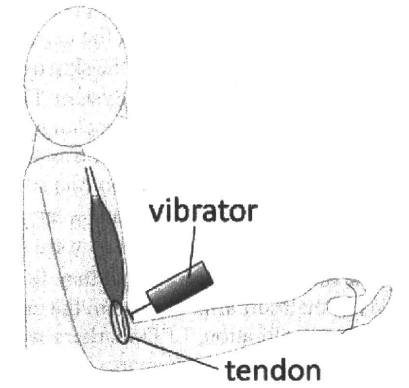

Fig. 1. Tendon vibration. A tendon is transcutaneously vibrated.

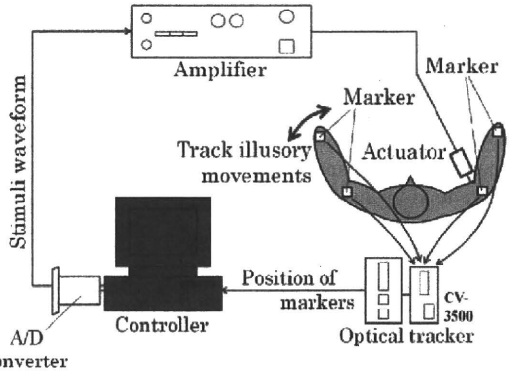

Fig. 2. Block diagram of the experiments. Tendons of right arm were vibrated. Participants moved their left forearm to show the velocity of the movement they felt in their right forearm. The arm positions were tracked optically to obtain angular velocity of forearms during vibration

This may imply that the central nervous system interprets the velocity to be zero based on the signals from the other Ia afferents. If this is true, a stimulation that activates numerous Ia afferents should evoke a sensation of rapid movement. In most studies, vibration was applied to a single tendon to evoke a sensation of a joint movement on one axis; however, generally several synergistic muscles are recruited for flexion or extension of a joint. Therefore, simultaneous vibration to synergistic muscles may evoke the sensation of a more rapid movement by activating Ia afferents of those muscles. Moreover, when a single tendon is vibrated, only some part of Ia afferents of the vibrated muscle generates an action

Manuscript received April 23, 2010. This work was supported in partly by Health and Labour Sciences Research Grant (H20-Nano-general-003) from the Ministry of Health, Labour and Welfare of Japan. Grant-in-Aid for Scientific Research (A) (20246045) from the Ministry of Education, Culture, Sports, Science and Technology

H. Yaguchi, O. Fukayama, T. Suzuki and K. Mabuchi are with The Graduate School of Information Science and Technology, The University of Tokyo, Tokyo, Japan (phone: 81-3-5841-6880, e-mail: Hiroaki_Yaguchi@ipc.i.u-tokyo.ac.jp).

potential per cycle[11]. Vibration to both ends of a muscle may produce greater activity because of more Ia afferents being stimulated, thereby resulting in a sensation of more rapid movement.

II. Methods

A. Experimental setup

Ten healthy volunteers participated in the experiment. Each participant was seated on a chair with his hands and forearms positioned horizontally on support tables.

Figure 2 shows a block diagram of the experiment system. Mechanical vibration was applied to the skin over the tendons. The vibration devices (Dia Medical System; DPS-270, Brüel & Kjaer; Type 1810) were driven by rectangular pulses. The peak-to-peak amplitude of the vibration was about 1 mm, the frequency was 100 Hz, and the duration was 10 s. Participants were instructed to close their eyes and wear headphones to prevent visual and auditory inputs. They were then instructed to indicate the movement velocity that they felt in their right arm by moving their left arm. To obtain the angular velocity of forearms during vibration, LED markers were attached to elbows and wrists of the participants, and these positions were tracked optically. The intensity of evoked kinesthesia was calculated by subtracting the angular velocity of the right arm from that of the left arm.

B. Vibration to both ends of a muscle

Vibration was applied to both ends of biceps brachii (BB) of 8 participants. While distal vibration was applied to the tendon, proximal vibration was applied to the muscle near the musclotendinous junction because the proximal tendons were located behind the other muscles. Vibration was applied to distal tendon and/or the proximal end 10 times each in a random order in 30 trials per participant. A rest interval of 3-4 min was provided after every 10 trials. After each rest interval and at the start of the experiment, it was confirmed that vibrations to either tendon evoked kinesthesia. A similar procedure was performed in the next experiment.

C. Vibration to synergistic muscles

Vibration was applied to the tendons of BB and brachioradialis muscle (BRM), both of which are synergists for elbow flexion. The distal tendons of BB and/or BRM were vibrated 10 times each in a random order in 30 trials per participant.

III. Results

A. Vibration to both ends of a muscle

Vibration to the distal tendon and/or proximal end of the BB evoked the sensation of a movement in all participants. The velocity of the illusory movement was 1.0 ± 0.7, 0.5 ± 0.4, and 1.7 ± 1.4 deg/s for the distal tendon, the proximal end, and both of the BB, respectively (Fig. 3). We conducted a Friedman test followed by a post-hoc Nemenyi test with vibration conditions ($\alpha = 0.05$). Significant differences were found between the vibration to the distal tendon or proximal end and to both.

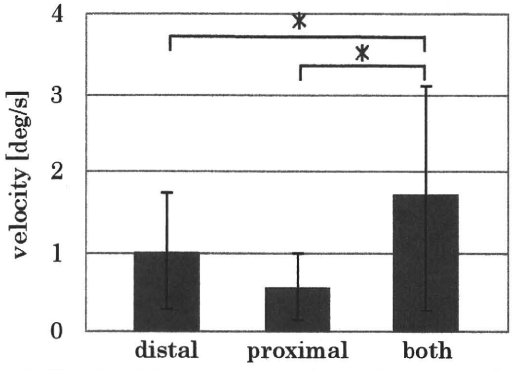

Fig. 3. Velocity of illusory movement induced by vibrating the distal tendon and/or proximal end of BB. The values are averaged over all participants. (*: $p < 0.05$)

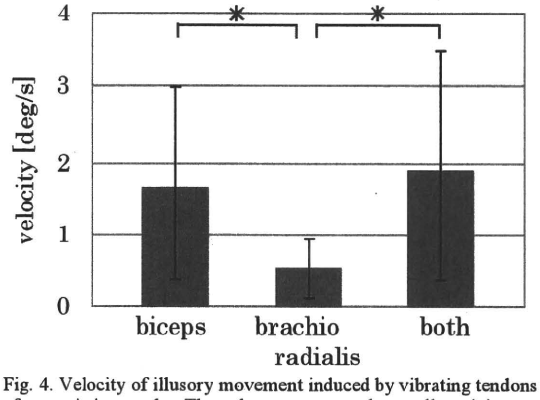

Fig. 4. Velocity of illusory movement induced by vibrating tendons of synergistic muscles. The values are averaged over all participants. (*: $p < 0.05$)

B. Vibration to synergistic muscles

Vibration to the distal tendons of BB and/or BRM evoked the sensation of a movement in all participants. The velocity of the illusory movement was 1.7 ± 1.3, 0.5 ± 0.4, and 1.9 ± 1.6 deg/s for BB, BRM, and BB + BRM, respectively (Fig. 4). As in the previous experiment, we conducted a Friedman test followed by a post-hoc Nemenyi test with vibration conditions ($\alpha = 0.05$). Significant differences in results were found between vibrations of BB and BRM, and between BRM and both.

IV. Discussion

Compared to vibration to the distal tendon or proximal end of biceps, vibration to both evoked a sensation of more rapid movement ($\alpha = 0.05$), although the velocity didn't reach that of large voluntary movements. This result seems to stem from increased activity of Ia afferents in the vibrated muscle. Tendon vibration activates not only Ia afferents but also cutaneous mechanoreceptors around the actuator. However, cutaneous receptors over the proximal end of the BB would not contribute to the kinesthesia of elbow movements,

because the skin over that end of the BB doesn't be transformed by elbow movements. Moreover, the activity of pacinian corpuscles, which are vibration receptors, impairs the ability to detect passive movements [12] at joints near the actuator. Illusory movement would not be induced by the activity of cutaneous mechanoreceptors incidental to tendon vibration.

However, the results did not indicate any significant difference between the velocities of illusory movements induced by the vibration to BB and to BB and BRM. This may be partly because BRM makes a smaller contribution to elbow flexion than BB, in which case the central nervous system would have less of a response to its signals.

V. Conclusion

We extended tendon vibration, with a focus on elbow extension, to evoke a sensation of more rapid movement. Compared to vibration to the distal tendon or proximal end of the biceps, vibration to both evoked a sensation of more rapid movement ($\alpha = 0.05$). However, the velocity didn't reach that of large voluntary movements. Stimulation methods that can evoke sensations of more rapid movement require further study.

References

[1] K. Warwick, M. Gasson, B. Hutt, I. Goodhew, P. Kyberd, B. Andrews, P. Teddy and A. Shad, "The application of implant technology for cybernetic systems," *Arch. Neurol.,vol.* 60, no. 10, pp. 1369-1373, 2003.

[2] G. S. Dhillon and K. W. Horch, "Direct neural sensory feedback and control of a prosthetic arm," *IEEE Trans. Neural Sys. Rehabil. Eng.*, vol. 13, no. 4, pp. 468-472, 2005.

[3] D. Burke, K. E. Hagbarth, L. Löfstedt and B. G. Wallin, "The responses of human muscle spindle endings to vibration of non-contracting muscles," *J. Physiol.*, vol. 261, pp. 673-693, 1976.

[4] D. Burke, K. E. Hagbarth, L. Löfstedt and B. G.Wallin, "The responses of human muscle spindle endings to vibration during isometric contraction," *J. Physiol.*, vol. 261, pp. 695-711, 1976.

[5] G. M. Goodwin, D. I. McCloskey and P. B. C. Matthews, "The contribution of muscle afferents to kinaesthesia shown by vibration induced illusions of movement and by the effects of paralysing joint afferents," *Brain*, vol. 95, pp. 705-748, 1972.

[6] J. P. Roll and J. P. Vedel, "Kinaesthetic role of muscle afferents in man, studied by tendon vibration and microneurogram," *Exp. Brain Res.*, vol. 47, pp. 177-190, 1982.

[7] D. F. Collins and A. Prochazka, "Movement illusion evoked by ensemble cutaneous input from the dorsum of the human hand," *J. Physiol.*, vol. 496, no. 3, pp. 857-871, 1996.

[8] D. F. Collins, K. M. Refshauge, G. Todd and S. C. Gandevia, "Cutaneous receptors contribute to kinesthesia at the index finger, elbow, and knee," *J. Neurophysiol.*, vol. 94, no. 3, pp. 1699-1706, 2005.

[9] E. Rabin and A. M. Gordon, "Prior experience and current goals affect muscle-spindle and tactile integration," *Exp. Brain Res.*, vol. 169, pp. 407-416, 2006

[10] G. Macefield, S. C. Gandevia and D. Burke, "Perceptual responses to microstimulation of single afferents innervating joints, muscles and skin of the human hand," *J. Physiol.*, vol. 429, pp. 113-129, 1990.

[11] J. B. Fallon and V. G. Macefield, "Vibration sensitivity of human muscle spindles and golgi tendon organs," *Muscle Nerve*, vol. 36, pp. 21-29, 2007.

[12] N.S. Weerakkody, J.L. Taylor and S.C. Gandevia, "The effect of high-frequency cutaneous vibration on different inputs subserving detection of joint movement," *Exp. Brain Res.*, vol. 197, pp. 347-355, 2009.

ト面は薔薇や無臭が噴射された時よりも硬く知覚された。また、滑らかな標準面と同時に薔薇が噴射されると、テスト面は無臭が噴射された時よりも滑らかに知覚された。これらの結果は、香りと感触の相互作用の存在を示すものであり、香りの種類によって影響を及ぼす感触が異なることが示唆された。

40. 到達把持運動が手指の身体近傍空間に及ぼす影響

渋谷賢（杏林大学・医・統合生理学）

本研究は、到達把持運動が手指の身体近傍空間に与える影響を調べた。被験者は物体への到達把持運動と伴に、運動開始前、開始直後、開始 0.2 秒後のいずれかに示指もしくは母指に加わる触覚刺激の選択反応課題を行った。触覚刺激と同時に物体上の LED が点灯したが、被験者はこの視覚刺激を無視した。運動開始前の反応時間は示指と母指の間に差を示さなかったが、開始直後と開始 0.2 秒後の反応時間は視覚刺激の同時呈示により示指の方が母指よりも有意に早くなった。この相違は視覚刺激が呈示される空間に依存し、把持物体の手前よりも奥の空間の方が大きかった。また，この相互作用は視線の移動に影響を受けなかった.

41. 視覚方位刺激の検出に及ぼす触覚フランカー刺激の文脈的修飾効果

和田裕一（東北大学情報科学研究科），三坂慎一郎（東北大学情報科学研究科）

ある方位を持った線分刺激やガボール刺激の検出に際して，同じ方位を持つフランカー刺激が同一線上の隣接する領域に存在している場合，当該刺激の検出が促進（場合によっては抑制）される（たとえば Polat & Sagi, 1993）。ここで，物体の輪郭情報は触覚によっても検知できる点を考慮すると，フランカー刺激が触覚に提示される場合でも，上述のような刺激布置条件を満たしていれば，視覚に提示される方位刺激の検出が促進される可能性が考えられる。そこで本研究では，視覚刺激の検出に及ぼす触覚フランカー刺激のクロスモーダルな文脈的修飾効果について検討した。

42. 腱振動刺激によって錯覚される運動の速度に関する研究

矢口博彬 (東京大学)、深山理 (東京大学)、鈴木隆文 (東京大学)、満渕邦彦 (東京大学)

腱振動刺激は、筋紡錘一次終末の活動を誘発し、関節運動の錯覚を引き起こす。しかし、錯覚される運動の速度は、高々数 deg/s と低速である。本研究では、高速な運動の錯覚が生じない原因として、腱振動刺激によって興奮するのは、その運動に関わる筋に分布する一次終末の一部に過ぎないことに着目した。興奮する一次終末の数を増加させるため 2 点の同時振動を行い、錯覚される運動の速度における影響を調べた。その結果、ひとつの筋の両端で同時に振動すると、その一方のみ振動する場合と比べ、高速な運動の錯覚を生じた。本発表では、以上の結果に加え、運動感覚生成の義手への応用に向けた取組みについて、併せて議論したい。

Print this Page

Presentation Abstract

Program#/Poster#: 782.12/PP8

Title: Neural representation of motion signal after direction remapping in touch: Evidence from motion aftereffect

Location: Halls B-H

Presentation Time: Wednesday, Nov 17, 2010, 11:00 AM -12:00 PM

Authors: *S. KUROKI[1,2], J. WATANABE[2], K. MABUCHI[1], S. TACHI[3], S. NISHIDA[2];
[1]The Univ. of Tokyo, Tokyo, Japan; [2]NTT Communication Sci. Labs., Kanagawa, Japan; [3]Keio Univ., Kanagawa, Japan

Abstract: The brain must realign information of tactile position and direction from the primary somatosensory maps to external coordinates in order to perceive the world appropriately. Although recent studies revealed sites of neural representations underlying remapping of positional information, a demonstration of neural representation for direction remapping was lacking. Here we psychophysically investigate whether the neural representation for direction remapping exists in the human tactile system using motion adaptation paradigm. We employed finger crossed posture to manipulate the relative spatial and somatotopic relations between fingers and compared the aftereffects of the inter-finger motions between normal and finger crossed posture. In normal posture, after adapting to a lateral motion between index and middle fingers, perceived motion direction was biased to the opposite direction to the adapted direction. In finger crossed posture, after adapting to the motion with the finger crossed, the posture was changed to normal one and test stimulus was presented. If the neural representation for direction remapping does not exist, the motion aftereffects could be observed in the somatotopic map, regardless of the postures. However, our results showed that the motion aftereffect was dominantly observed in the external coordinate, namely the perceived direction after adaptation is the same as the adapted direction in the somatotopic map. These findings firstly demonstrate the existence of neural representation for remapped motion direction, and in addition, imply that tactile